

Article

Uncertainty Analysis of Remote Sensing Pretreatment for Biomass Estimation on Landsat OLI and Landsat ETM+

Qi Zhang ¹ , Lihua Xu ^{1,2,*}, Maozhen Zhang ¹, Zhi Wang ¹, Zhangfeng Gu ², Yaqi Wu ², Yijun Shi ²  and Zhangwei Lu ²

¹ School of Environment and Resources Science, Zhejiang A & F University, Hangzhou 311300, China; 2017103241003@student.zafu.edu.cn (Q.Z.); zhangmz@zafu.edu.cn (M.Z.); 2018103242004@stu.zafu.edu.cn (Z.W.)

² School of Landscape Architecture, Zhejiang A & F University, Hangzhou 311300, China; 2019105041001@stu.zafu.edu.cn (Z.G.); 20030050@zafu.edu.cn (Y.W.); yijun_shi@zafu.edu.cn (Y.S.); zhwlu@zafu.edu.cn (Z.L.)

* Correspondence: xulihua@zafu.edu.cn; Tel.: +86-138-0579-9690

Received: 16 December 2019; Accepted: 13 January 2020; Published: 15 January 2020



Abstract: The accurate quantification of biomass helps to understand forest productivity and carbon cycling dynamics. Research on uncertainty during pretreatment is still lacking despite it being one of the major sources of uncertainty and an essential step in biomass estimation. In this study, we investigated pretreatment uncertainty and conducted a comparative study on the uncertainty of three optical imagery preprocessing stages (radiometric calibration, atmospheric and terrain correction) in biomass estimation. A combination of statistical models (random forest) and multisource data (Landsat enhanced thematic mapper plus (ETM+), Landsat operational land imager (OLI), national forest inventory (NFI)) was used to estimate forest biomass. Particularly, mean absolute error (MAE) and relative error (RE) were used to assess and quantify the uncertainty of each pretreatment, while the coefficient of determination (R^2) was employed to evaluate the accuracy of the model. The results obtained show that random forest (RF) and 10-fold cross validation algorithms provided reliable accuracy for biomass estimation to better understand the uncertainty in pretreatments. In this study, there was a considerable uncertainty in biomass estimation using original OLI and ETM+ images from. Uncertainty was lower after data processing, emphasizing the importance of pretreatments for improving accuracy in biomass estimation. Further, the effects of three pretreatments on uncertainty of biomass estimation were objectively quantified. In this study (results of test sample), a 33.70% uncertainty was found in biomass estimation using original images from the OLI, and a 34.28% uncertainty in ETM+. Radiometric calibration slightly increased the uncertainty of biomass estimation (OLI increased by 1.38%, ETM+ increased by 2.08%). Moreover, atmospheric correction (5.56% for OLI, 4.41% for ETM+) and terrain correction (1.00% for OLI, 1.67% for ETM+) significantly reduced uncertainty for OLI and ETM+, respectively. This is an important development in the field of improving the accuracy of biomass estimation by remote sensing. Notably, the three pretreatments presented the same trend in uncertainty during biomass estimation using OLI and ETM+. This may exhibit the same effects in other optical images. This article aims to quantify uncertainty in pretreatment and to analyze the resultant effects to provide a theoretical basis for improving the accuracy of biomass estimation.

Keywords: biomass estimation; uncertainty; data preprocessing; 10-fold cross validation; random forest

1. Introduction

The importance of forest ecosystem services function has been universally acknowledged, especially as it plays an important role in maintaining global carbon balance. The conversion of forestry may increase carbon emissions, thereby influencing global climate and changes in other environmental factors [1–5]. Forests account for about 90% of global terrestrial vegetation biomass. For this reason, biomass estimation is considered a key measure of ecosystem productivity and an indicator of the carbon sequestration capacity in a forest. As a result, it is used for quantifying the role of forests in the carbon cycle, energy production, and carbon stock estimation during climate change modelling [6–12].

In general, forest biomass is divided into aboveground biomass (AGB) and below-ground biomass (BGB) [13]. Studies estimating biomass have traditionally focused on AGB segment due to the difficulty of collecting field survey data for BGB [14]. In this study, the term forest biomass is used to denote forest AGB [13]. The estimation of AGB helps to study plant productivity, carbon cycles, nutrient allocation, and fuel accumulation in terrestrial ecosystems [15–18]. Currently, various techniques have been developed to estimate forest biomass. Among them, on-site measurement is the most accurate method, and hence it is preferred [19,20]. However, it is not feasible because it is labor intensive and expensive [21–23]. To circumvent the aforementioned problems while ensuring the accurate and affordable measurement of forest biomass on a large spatial scale, remote sensing and sample survey data approaches have been proposed [24–26].

The forest is a material space composition, and thus the estimation of its biomass through remote sensing poses a spatial problem. For instance, spatial estimation produces analog values of the forest biomass estimation simulation system, with an erroneous true value. It can only be close to the true value under certain conditions. Uncertainty, which is a concept of inaccuracy, fuzziness and ambiguity [27], represents the distribution of differences between a true value and a range of estimates, and is normally given at a particular confidence level [28]. In general, forest biomass estimates acquired through remote sensing will have different sources of errors emanating from estimation models, ground survey data, and pre-processing [29–31]. Further, multitemporal optical wavelength satellite data acquired under different acquisition conditions and using different sensors may have uncertainty in biomass estimation due to a variety of factors, including: (1) atmospheric and cloud contamination [32,33], (2) changes in geometry of the sun-surface sensors [34,35], (3) spectral bandpass and spatial resolution differences of the sensors [36,37], (4) sensor degradation and calibration changes [11], and (5) reflectivity inconsistency and data processing issues [38,39]. Accurate knowledge of uncertainties resulting from the aforementioned sources is therefore essential for accurate biomass estimation as it improves the quality of data [40]. Remote sensing has numerous advantages, although its accuracy in biomass estimation deserves further improvement. In particular, more robust and comprehensive estimates of uncertainty in biomass estimation are needed [28]. Previous research on the uncertainties of forest biomass has reported success in the following: (1) estimation models [41,42], (2) ground survey data [43], (3) differences in satellite sensors [44], (4) error transmission [45], (5) differences in spatial resolution [36], and (6) sampling [46,47].

Landsat sensors are frequently used to predict forest biomass and carbon storage, mainly because data from the platform are freely downloadable with a long history and moderate spatial resolution [39]. For instance, Cyrus et al. [48] used Landsat TM and Enhanced Thematic Mapper-Plus (ETM+) to estimate biomass in southern Africa while Zheng et al. [49] produced age and AGB maps using both Landsat ETM+ and field-measured stand level data. Similarly, National Aeronautics and Space Administration (NASA) successfully launched the operational land imager (OLI) and thermal infrared sensor (TIRS) in 2013, continuing Landsat's legacy. In addition, Chenge et al. [50] used Landsat 8 OLI data to map tree AGB and carbon stock in Omo Forest Reserve, Nigeria. By linking Landsat 8 and forest inventory data, Belachew et al. [51] successfully (1) developed linear mixed effects models for total living biomass (TLB) estimation as a function of spectral variables, (2) developed a 30-m resolution map of the total living carbon (TLC), and (3) estimated the total TLB stock of the study area. A series of Landsat satellites are employed to estimate biomass in large areas using remote sensing.

For this reason, users of the technology have developed a keen interest in its accuracy for biomass estimation. Consequently, studies have reported uncertainties from different sources such as surface net radiation [52], regression models [53,54], atmospheric corrections [55], and the absolute radiometric calibration [56] of Landsat. However, knowledge on uncertainties emanating from pretreatment is lacking. The pretreatment of Landsat is mostly divided into geometric correction, radiometric calibration, as well as atmospheric and terrain corrections [57]. Markham et al. [58] reported that radiance calibration was performed with an uncertainty of about 3% while the reflectance calibration had an uncertainty of about 2%. Biomass estimation uses spectral information of the satellite, and the uncertainty of the pre-processed spectral information from the satellite is used to determine the uncertainty during biomass estimation. However, quantitative research on this uncertainty during pretreatment is limited. Varying pretreatments often result in different datasets and this is one major source of uncertainty during biomass estimation. The accurate quantification of the uncertainty of preprocessing is helpful as it can improve the process during remote sensing using Landsat. Apart from selecting a suitable pretreatment, it is also critical to use appropriate methods to quantify uncertainty during biomass estimation. For instance, Fu [30] reported the use of Monte Carlo simulation in a traditional model analysis that was conducted to estimate AGB on a regional scale and to assess the corresponding uncertainties contributed separately by sampling and model errors. Similarly, Zhang et al. [59] evaluated the uncertainty of five K-factor prediction models using statistics such as MAE, mean relative error (MRE), root mean squared error (RMSE) and accuracy factor (A_f) in seven typical soils in subtropical China. Furthermore, Li [60] used RE to evaluate the uncertainties of simulating crop growth and yield estimates due to different assimilation strategies and multi-source errors. The confidence of RE and MAE have long been recognized as an important index for evaluating uncertainty.

Exploring the influence of pretreatment on uncertainties associated with using Landsat images to estimate biomass will help to generate a practical guide for researchers for accurate biomass estimation.

The remaining part of this research proceeds as follows: details of materials, data and methods are described in Section 2. In Section 3, the uncertainty statistics of each pretreatment stage and the R^2 of the model are depicted. We discuss the mechanisms behind some of the phenomena in this work and summarize the conclusions in Sections 4 and 5, respectively.

2. Materials and Methods

2.1. Study Area

Kaihua county ($28^{\circ}54' - 29^{\circ}30' N$, $118^{\circ}01' - 118^{\circ}37' E$) is located in Zhejiang province, China. It is a typical relief terrain of a mountainous area, mainly subtropical evergreen species and including a forest area coverage of 80.54%. It is known as the “Amazon rainforest of China”. The terrain of Kaihua county is affected by geological tectonic movement, and the terrain is uplifted and obviously cut. Most of the valleys are deep and v-shaped, and the narrow slopes are steep, which can better highlight the terrain correction effect.

2.2. Landsat Data

Landsat 8 OLI data and Landsat 7 ETM+ data (path 120, row 40; Table 1) processed to level L1T were acquired from the United States Geological Survey (USGS; <http://earthexplorer.usgs.gov/>). The spectral bands used in this study included blue (0.45–0.51 μm), green (0.53–0.59 μm), red (0.64–0.67 μm), near infrared (NIR; 0.85–0.88 μm), shortwave infrared 1 (SWIR 1; 1.57–1.65 μm), and SWIR 2 (2.11–2.29 μm). There is some overlapping time period between ETM+ and OLI. Using different sensors of Landsat is better to understand the influence of pretreatment on uncertainties of biomass estimation using Landsat.

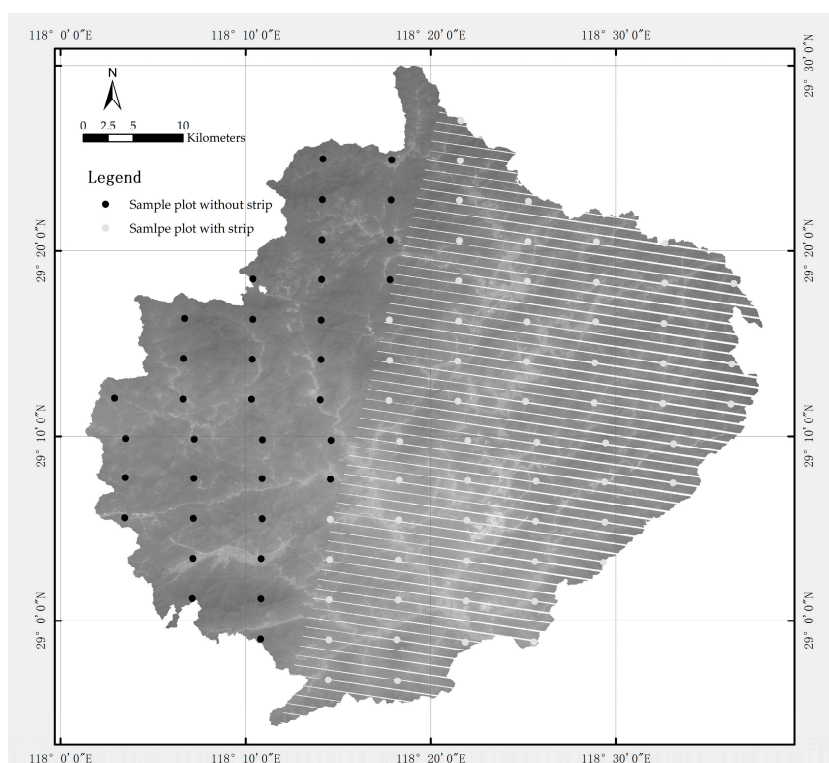
Table 1. Remote sensing data used in this study. MS—multispectral.

Remote Sensing Data	Date	Pixel Size
Landsat 8 OLI	14 October 2013	MS: 30 m
Landsat 7 ETM+	22 October 2013	MS: 30 m

2.3. Field Data

National forest resource assessment and monitoring are commonly known as the national forest inventory (NFI). In many countries, NFI has become an important part of the national information infrastructure [61–64]. In China, the NFI was started in 1973, and has been widely recognized as a powerful and appropriate dataset for calculating forest biomass on a large scale [65–69]. The NFI has been conducted nearly every five years since the late 1970s and the eighth NFI was conducted for the period 2009–2013 [70]. All provinces are now using a systematic sampling design and permanent field plots. The permanent plots in Zhejiang province were established through the 4 × 6 km grid, from 0.08 ha in each plot size (28.28 × 28.28 m). This study used the eighth NFI (2014 NFI). A total of 96 sample plots were evenly distributed in the study area, and 35 plots without strip were distributed. We assumed that the data from sample plots was the true value of biomass (range of biomass from 0 to 284.22 t/ha).

We noted that ETM+ was damaged by scan lines corrector (SLC) failure on 31 May 2003. The data strip was lost, and the image was seriously striped. To control variables as much as possible and to reduce interference and influence factors, we selected 35 sample plots without strip as sample data (Figure 1). Consequently, the sample plot location was basically consistent, compared to the actual data after geometric correction.

**Figure 1.** Sample plot.

2.4. Experimental Scheme

Based on the Landsat (OLI, ETM), we carried out pre-treatment uncertainty research on biomass estimation, then evaluated and quantified effects of different pretreatments on the uncertainty of biomass

estimation using Landsat images. We selected two scenes images, OLI and ETM+, as the original remote sensing data, and used the same geometric correction, radiometric calibration, atmospheric correction (FLAASH), and terrain correction (C-correction) preprocessing for the images. After a stage of pre-processing, the original image data was used to estimate biomass and calculate RE, MAE, and R^2 of the estimated biomass and biomass true values. The difference in RE between each stage and the previous pretreatment stage is the uncertainty of biomass estimation.

2.5. Random Forest Modeling

RF is a machine-learning approach based on decision trees that has been shown to provide high prediction accuracy for biomass estimation [71–76]. RF avoids the overfitting problem in decision tree learning and has a high tolerance to noise and outliers. We used the RF machine learning algorithm as implemented in the R package randomForest [77]. In this study, 2000 trees (ntree) were used in the RF modeling. For the parameter mtry (i.e., the number of variables to be tested at each node), the default value of the square root of the total number of predictor variables was used [71]. The parameter node-size was set to the value of 5.

2.6. Remote Sensing Predictor Variables

In this paper, by referring to the literature, 5 kinds of vegetation indexes were selected for biomass estimation (Table 2). All the vegetation indexes were used to estimate AGB. We built a regression model based on the dataset of NFI and the vegetation indices. The vegetation indices were used as the independent variables for regression model.

Table 2. Summary of the spectra predictor variables included in predictive modeling of AGB.

Predictor Variables	Formula
Normalized Difference Vegetation Index (NDVI) [78]	$(\text{NIR} - \text{Red}) / (\text{NIR} + \text{Red})$
Generalized Difference Vegetation Index (GNDVI) [79]	$(\text{NIR} - \text{Green}) / (\text{NIR} + \text{Green})$
Soil-Adjusted Vegetation Index (SAVI) [80]	$(1 + 0.5) \times \frac{\text{NIR} - \text{Red}}{\text{NIR} + \text{Red} + 0.5}$
Modified Soil-Adjusted Vegetation Index (MSAVI) [81]	$\frac{2 \times \text{NIR} + 1 - \sqrt{(2 \times \text{NIR} + 1)^2 - 8 \times (\text{NIR} - \text{Red})}}{2}$
Enhanced vegetation index (EVI) [82]	$2.5 \times \frac{\text{NIR} - \text{Red}}{\text{NIR} + 6 \times \text{Red} - 7.5 \times \text{Blue} + 1}$

NIR, red, blue and green are the reflectance of bands. NIR is near infra-red band, red is the red band, green is the green band, and blue is the blue band.

2.7. Accuracy Assessment and Evaluation Indicators

The predictive ability of all models was assessed using 10-fold cross validation (10% of reference data). That is, in each round of biomass estimation, the data (data of sample plot and remote sensing variables) was divided into 10 parts. Select one from them as the testing samples, and the rest will be regarded as training samples. Then, 10 trainings shall be conducted in sequence. In each round, ten results of each evaluation index were obtained, and the average value was taken as the final result. The cross-validation approach is based on the entire reference dataset, rather than using separate training and validation data subsets, which is a useful approach when there is limited reference data [83]. To ensure the authenticity and reliability of the data, the study was cycled for 100 rounds. Three measures of biomass estimation accuracy were calculated from the 10-fold cross validation, including R^2 , MAE, and RE.

2.8. Variance

In this study, we sought to evaluate the uncertainties of biomass estimation at pretreatment using Landsat 8 OLI and Landsat 7 ETM+ images based on the two indices (RE and MAE).

Landsat remote sensing image preprocessing is divided into four stages: geometric correction, radiation calibration, atmospheric correction, and terrain correction. In this study, the OLI and ETM+

original images and the results of radiation calibration, atmospheric correction, and terrain correction were used to estimate biomass to better analyze the uncertainty of biomass estimation. Further, the RE, MAE, and model precision (R^2) of the estimated biomass and the actual biomass of the sample land at each stage were calculated. The relative error of each stage is the uncertainty of remote sensing biomass estimation in this stage. The uncertainty caused by different pretreatments can be measured by calculating the difference between the relative error of the previous stage pretreatment results. Results were subjected to statistical analysis.

$$R^2 = \frac{\sum_{i=1}^n (y_i - \bar{y}_i)^2 (\hat{y}_i - \bar{\hat{y}}_i)^2}{\sum_{i=1}^n (y_i - \bar{y}_i)^2 \sum_{i=1}^n (\hat{y}_i - \bar{\hat{y}}_i)^2} \quad (1)$$

$$MAE = \frac{\sum_{i=1}^n |\hat{y}_i - y_i|}{n} \quad (2)$$

$$RE = \frac{\sum_{i=1}^n |\hat{y}_i - y_i|}{n \times y_i} \quad (3)$$

where y_i is plot biomass value, \hat{y}_i is the predicted plot biomass value, \bar{y}_i is the average of y_i , $\bar{\hat{y}}_i$ is the average of \hat{y}_i , and n is the number of samples.

3. Results

3.1. Biomass Estimation from Raw Data

The R^2 value from biomass estimation results for ETM+ and OLI original images is described by a fold line diagram Figure 2a,b. The results show that: (a) the original biomass estimated using OLI images had a higher overall accuracy than ETM+ (OLI: 0.86~0.88, ETM+: 0.84~0.85); (b) accuracy of the two models showed a sharp fluctuation following an even distribution of the high, medium, and low values (OLI: 0.0001~1, ETM+: 0.000007~1). The accuracy of biomass estimation using remote sensing models based on OLI and ETM+ raw image data was unstable, as 23% and 24% were less than mean 1 standard deviation (SD), respectively (Table 3). The MAE of biomass estimation for ETM+ and OLI original images is described using a fold line presented in Figure 2c,d. The results of ETM+ and OLI were approximate. (c) In OLI, based on a training sample of 24.48~25.03 t/ha, a mean value of 24.73 t/ha, and biomass estimation uncertainty of about 21.05% were recorded. In ETM+, a training sample of 25.19~25.74 t/ha resulted in an average value of 25.47t/ha with an uncertainty of about 23.48%. (d) The MAE of both OLI and ETM+ showed a large fluctuation with a relatively large number of outliers. In OLI, a mean value of 47.1 t/ha with an uncertainty of about 33.70%, results had 15 rounds with values of MAE greater than mean 1 standard deviation. In ETM+, a mean value of 50.3 t/ha with an uncertainty of about 34.28%, results had 14 rounds with values of MAE greater than mean 1 standard deviation. Compared with Figure 2b, we found that the high MAE value corresponded to the low R^2 value of the test sample. The MAE showed a negative correlation with R^2 and was highly disturbed by R^2 change. In summary, biomass estimation for OLI and ETM+ raw data was not entirely accurate, with results showing high uncertainty. MAE showed a negative correlation to R^2 .

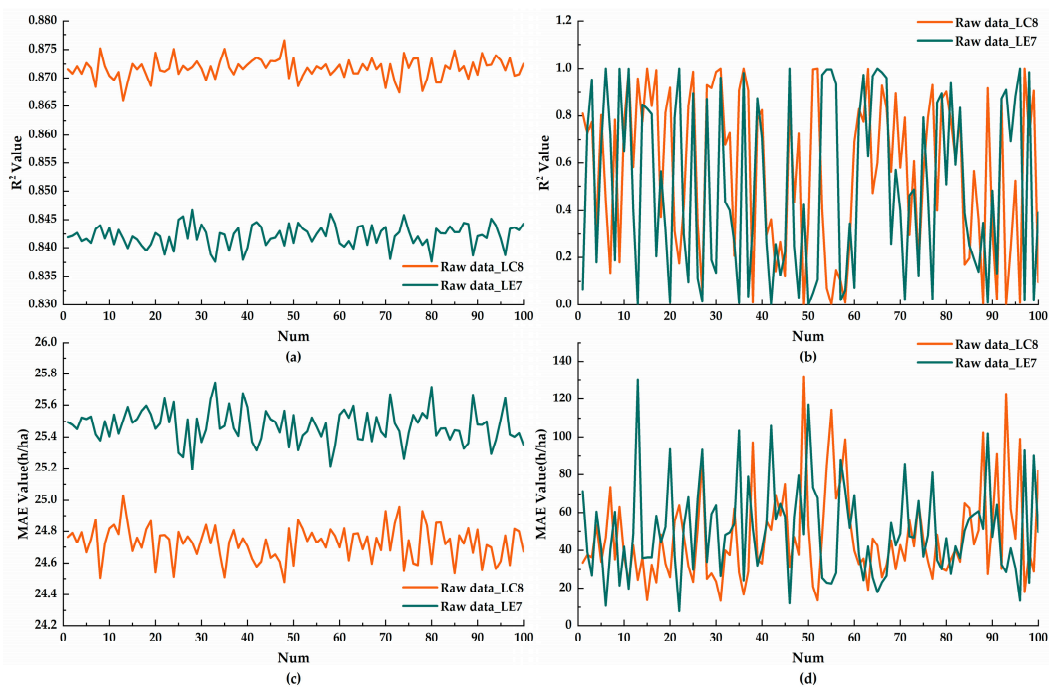


Figure 2. The R^2 and MAE of ETM+ and OLI biomass estimation results for the original image. (a,c) Results of training samples; (b,d) Results of test samples.

Table 3. Summary of the R^2 and MAE of test samples included in each stage.

Class	Value	Original Image		Radiometric Calibration		Atmospheric Correction		Terrain Correction	
		OLI	ETM+	OLI	ETM+	OLI	ETM+	OLI	ETM+
R^2	Mean	0.571	0.499	0.565	0.498	0.670	0.561	0.725	0.681
	SD	0.332	0.364	0.329	0.343	0.304	0.337	0.270	0.323
	<SD	23	24	22	23	18	21	18	21
MAE	Mean	47.1	50.3	49.4	54.2	44.0	45.3	42.8	43.3
	SD	24.3	25.3	24.2	24.9	21.1	24.6	21.2	20.7
	>SD	15	14	14	14	14	12	14	13
	<SD	7	15	11	16	12	20	17	22

SD is standard deviation, <SD indicate the number of rounds with values of R^2 /MAE less than mean 1 standard deviation, >SD indicate the number of rounds with values of MAE greater than mean 1 standard deviation.

3.2. Biomass Estimation from Radiometric Calibration

R^2 results in biomass estimation following radiometric calibration of the ETM+ and OLI images are presented in Figure 3a,b. The results show that: (a) R^2 from both ETM+ and OLI had a slight downward trend with a high fold line. Particularly, OLI decreased to between 0.84 and 0.85 while that in ETM+ decreased to 0.83 to 0.84. (b) In addition, the accuracy of the two models showed a marked fluctuation (OLI: 0.0001~1, ETM+: 0.00004~1). Despite this instability in model accuracy, the mean value showed a small increase, and comparison with the original images showed a lower frequency and an improved trend. Details can be found in Table 3, the SD did decrease. These findings indicate that radiometric calibration slightly reduced the accuracy of the OLI and ETM+ biomass estimation models but still maintained high accuracy.

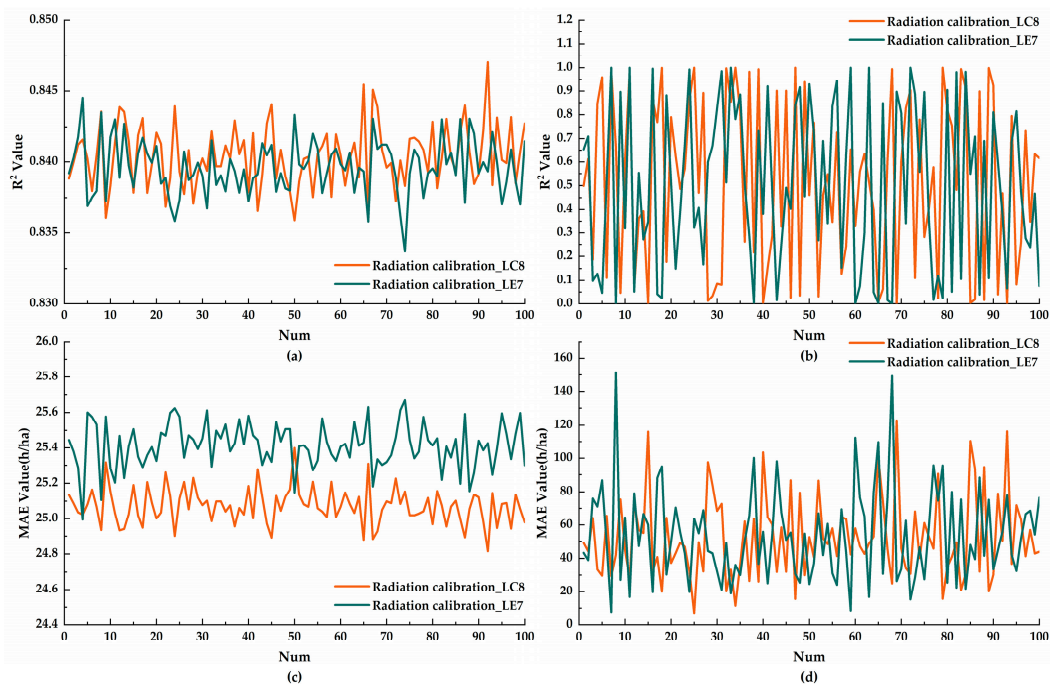


Figure 3. The R^2 and MAE of ETM+ and OLI biomass estimation results after using Radiometric Calibration. (a,c) Results of training samples; (b,d) Results of test samples.

A further analysis of the MAE of biomass estimation following radiometric calibration yielded similar results between ETM+ and OLI (Figure 3c,d). A comparison with the original image results showed a slight but not significant MAE uncertainty. In OLI (24.82~25.40 t/ha), a mean value of 25.07 t/ha and a biomass estimation uncertainty of about 21.67% under radiometric calibration were recorded accounting for a 0.62% increase. For ETM+ (25.00~25.67 t/ha) the mean MAE value was 25.41 t/ha with an uncertainty of about 24.42%. This indicated a 0.94% increase in large fluctuations as well as abnormal values, recorded between them as well as a negative correlation to R^2 . When compared to results from the original images, the frequency of abnormal values decreased and the number of rounds with values of MAE less than mean 1 SD was increased. In addition, the abnormal value of test samples decreased while its stability increased. For OLI, the mean MAE value was 49.4 t/ha with an uncertainty of about 35.12% being recorded, accounting for a 1.38% increase. In ETM+, the uncertainty ratio was 36.36%, accounting for a 2.08% increase. These observations indicate that, after radiometric calibration, the MAE and uncertainty of biomass estimation show a slight but not significant increase.

3.3. Biomass Estimation after Using Atmospheric Correction

Analysis of R^2 in biomass estimation following atmospheric correction showed a slight increase in R^2 as well as improved model accuracy in both ETM+ and OLI (Figure 4a,b). (a) Models recorded a significant increase in their range with 0.87~0.88 and 0.85~0.86 for OLI and ETM+, respectively. When compared with results from biomass estimation following radiometric calibration, atmospheric correction effectively improved the accuracy of the model. (b) We also observed a reduction in two ranges (OLI: 0.024~1; ETM+: 0.00029~1). In addition, the low-value frequency reduced, with a moderately high distribution 0.4~1. For both OLI and ETM+, the mean value was increased, SD and "> SD" were decreased (Table 3). In the range of 0.6~1.0, the number of rounds was increased significantly. Generally, this indicated that atmospheric correction effectively improved the accuracy of the model compared to radiometric calibration.

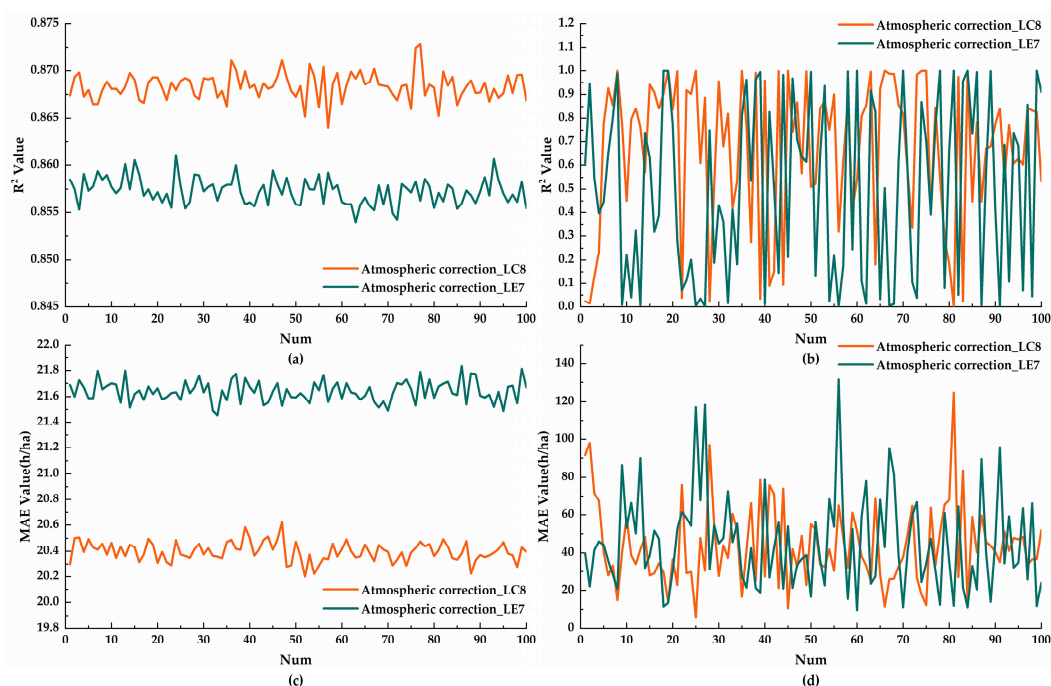


Figure 4. The R^2 and MAE of ETM+ and OLI biomass estimation results after using Atmospheric Calibration. (a,c) Results of training samples; (b,d) Results of test samples.

The MAE of biomass estimation after using atmospheric correction showed a downward trend with a reduction in uncertainty (Figure 4c,d). The results show that: (c) A range reduction was observed in OLI at 20.20~20.62 t/ha with a mean value of 20.40 t/ha. The uncertainty of biomass estimation after using atmospheric correction was about 17.89%, which was 3.78% lower. In ETM+, the range decreased to 21.45~21.84 t/ha with a mean value of 21.64 t/ha. Its uncertainty was about 20.70% representing a significant decrease of 3.72%. (d) The uncertainty of OLI test samples was about 29.56%, about 5.56% lower. In ETM+, the uncertainty was about 31.95%, about 4.41% lower. The abnormal values decreased. Compared with radiometric calibration results, the number of MAE (less than 40) increased significantly. The mean values were 44.0 t/ha and 45.3 t/ha from OLI and ETM+, respectively, reduced significantly. Further, the number of rounds with values of MAE less than mean 1 SD was increased, that is, the lower the MAE, the higher the accuracy. These findings indicate that atmospheric correction can effectively reduce the uncertainty of OLI and ETM+.

3.4. Biomass Estimation Following Terrain Correction

R^2 values of biomass estimation, after terrain correction, are represented by a line chart (Figure 5a,b). Results show that: (a) After using terrain correction, the change in accuracy tends to be stable, which is basically consistent with the atmospheric correction results of 0.87~0.88 and 0.85~0.86 for OLI and ETM+, respectively; (b) the frequency of low values was significantly reduced, while that of high values (greater than 0.6) increased significantly. The mean value was also increased and the number of rounds with values of R^2 less than mean 1 SD was decreased (Table 3), signifying an increasing trend of accuracy. In summary, terrain correction effectively improved the accuracy of model.

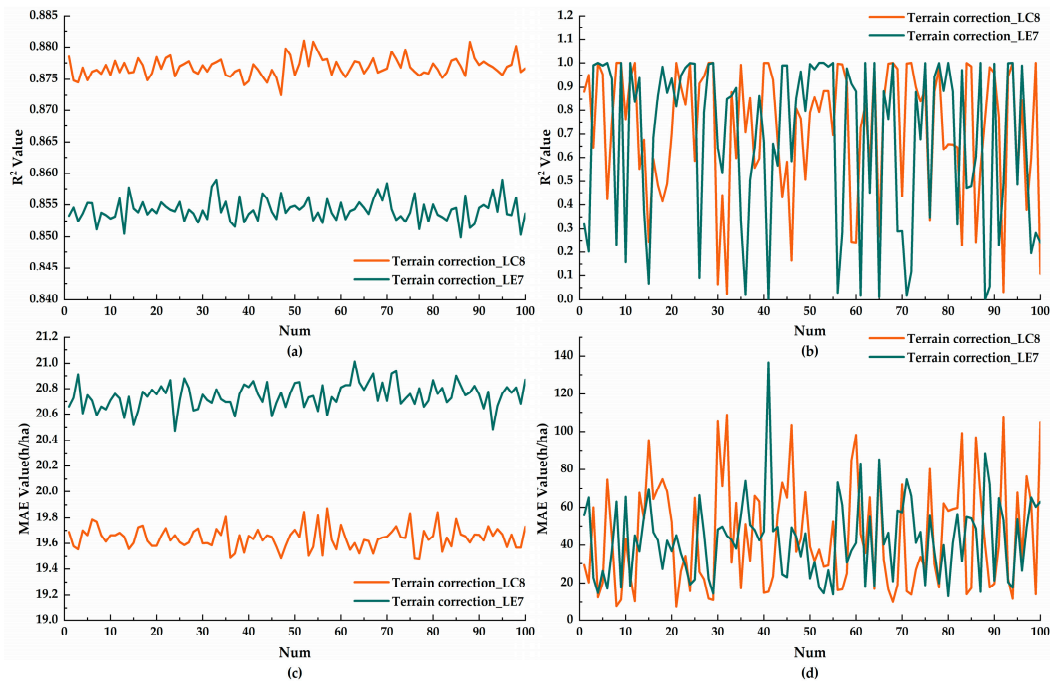


Figure 5. The R^2 and MAE of ETM+ and OLI biomass estimation results after using terrain calibration. (a,c) Results of training samples; (b,d) Results of test samples.

Analysis of MAE after using terrain correction showed a constant downward trend with a decreased uncertainty of biomass estimation and this was relatively lower compared with what was observed after atmospheric correction (Figure 5c,d). Particularly, the results show that: (c) a reduced MAE range of 19.48–19.87 t/ha and an average of 19.64 t/ha was recorded in OLI. Similarly, the uncertainty of biomass estimation using remote sensing after terrain correction was about 16.81%, which was 1.08% lower than for atmospheric correction. In ETM+, the MAE range reduced to 20.47–21.01 t/ha with a mean value of 20.74 t/ha, representing a 2.42% reduction; (d) the frequencies of high and abnormal values as well as uncertainty decreased significantly. It was concluded from the results obtained in Table 3, that the mean and SD were decreased, with the number of rounds with values of MAE less than mean 1 SD increased. The terrain correction greatly improved overall accuracy. Likewise, we observed 28.56% and 30.28% uncertainty in biomass estimation from OLI and ETM+, respectively. Under terrain correction, that was reduced by 1.00% and 1.67%. In summary, these results showed that terrain correction can effectively reduce the uncertainty of biomass estimation for OLI and ETM+ during remote sensing.

4. Discussion

Although numerous studies on forest biomass estimation have been conducted, substantial uncertainties remain in their current estimations. In this study, we analyzed the effects of the pretreatment (three stages) on the uncertainty of biomass estimation from optical remote sensing data. The MAE and RE were used to assess and quantify the uncertainty of each pretreatment, and R^2 further analyzed to evaluate model accuracy.

In recent years, random forest has gained popularity as an effective classification method in the remote sensing domain [84–86]. Results from our study additionally confirm that the random forest ensemble is a robust and accurate method for regression type applications as well.

A comparative analysis of our findings showed that the estimation of forest biomass based on the 10-fold cross validation method has a high model accuracy, and this accurately reflects the different influence of each pretreatment on the uncertainties observed from OLI and ETM+. In this study, original images of OLI and ETM+ for biomass estimates had 21.05% and 23.45% uncertainties

in the training sample, respectively, and uncertainly with 33.70% and 34.28% in the test sample. Several design enhancements have been made in OLI relative to prior Landsat instruments. These enhancements include pushbroom imaging which provides substantially improved signal to noise ratio (SNR), spectral bandpasses refinement to avoid atmospheric absorption features, 12 bit data resolution that provides a larger dynamic range for limiting levels of saturation and increasing SNR, as well as a set of well-designed onboard calibrators to monitor the stability of the sensor [87]. For this reason, the OLI original image has a lower uncertainty than that of ETM+ during biomass estimation.

Radiometric calibration resulted in a slight decrease in accuracy of OLI and ETM+ models, an unchanged MAE, and a slight increase in uncertainty of biomass estimation. Markham et al. [58] explored the effect of radiance calibration uncertainty which further reduced to about 2% following reflectance calibration. When receiving solar radiation and converting it into DN values, the Landsat sensor is prone to oversaturation due to the limitation of data bit width (OLI: 12 bit, ETM+: 8 bit). It is possible that this is the reason why ETM+ results in greater uncertainty than OLI. In this study, we considered that radiometric calibration converts the original image DN value into a radiance value. The reflectivity process is affected by its uncertainty and the possible supersaturation of the original data. This, in turn, leads to an increase in the uncertainty of biomass estimation, although the change is small. Radiometric calibration results in increase in instability of accuracy in a test sample model to a certain extent compared with the original image. This has less influence on the uncertainty of biomass estimation.

Atmospheric correction can eliminate the influence of factors, including the atmosphere and illumination on surface reflection. This leads to lead to more accurate physical model parameters such as surface reflectivity and radiation brightness. Ghulam et al. [88] used 6S atmospheric correction to reduce uncertainties in electromagnetic wave transmission and effectively eliminate perturbations from geometric and system corrected ETM+ imagery. Other reports have demonstrated that, after atmospheric correction, the results of MAE are significantly lower than those of radiometric calibration, and the accuracy of the model is significantly improved [89,90]. In the current study, the uncertainty in both models significantly decreased, indicating that the atmospheric correction effectively improved estimation accuracy and reduced the uncertainty of biomass estimation using Landsat. Zhu et al. [91] proposed that improved atmospheric correction and surface reflectance removal schemes may decrease the uncertainty generated by water surface. Based on our results, we conclude that the improved atmospheric correction method is the most effective for further reduction of uncertainty during biomass estimation.

Furthermore, the findings of the current study showed that MAE and uncertainty of biomass estimation from OLI and ETM+ remote sensing showed a similar trend after terrain correction as those recorded following atmospheric correction. The accuracy was also stable. However, terrain correction resulted in a significantly higher effect on reduction of uncertainty in ETM+ biomass estimation compared to OLI. Images used in this study were selected at a close time, but there was an eight-day time difference. The alpine area of this study was undulating, and the valleys were mostly steep with a "V" shape. Although this better reflected the terrain correction effect, it also shows that this effect is more susceptible to imaging conditions. Analysis and subsequent comparison of the imaging parameters in the sensor revealed that ETM+ has better imaging conditions with a higher solar elevation angle than OLI, which may lead to a better ETM+ effect in terrain correction and lower uncertainty of biomass estimation.

Our results further indicated that pre-processing improved the accuracy of the biomass estimation model relative to the previous stage. The R^2 changes tended to be stable after terrain correction, which is consistent with previous reports [92]. Further, MAE was negatively correlated with R^2 , and the uncertainty of biomass estimation also decreased, indicating that improving model accuracy is helpful in reducing the uncertainty of biomass estimation.

Although we predicted that the three pretreatments can exhibit the same effects of uncertainty during biomass estimation in other optical images. In this study, we used only one correction model for

each pretreatment. Differences in the selection of the correction model for pretreatment may produce different effects, thus affecting the performance of reducing the uncertainty of biomass estimation. We should investigate more attempts in the future to understand the impact of different correction models. In addition, we assumed that the data from sample plots was the true value of biomass. Actually, there is an inevitable measurement error between the data of sample plots and true value, and it is unpredictable and unavoidable. The numerical values of uncertainty may have some differences. The amount of sample plots in a study area may also influence the evaluation results. The datasets from Landsat are easy to acquire and use. More effort is needed to better understand the behavior at pretreatment.

5. Conclusions

Remote sensing techniques have many advantages, in biomass estimation, over traditional field measurement methods and provide the potential to estimate biomass at different scales. However, there is still a need for improving the accuracy of biomass estimates [93,94]. Based on the adjacent time OLI, ETM+ images, and 2014 NFI data, we used the RF model and 10-fold cross validation method to determine the effects of different pretreatments on the uncertainty of biomass estimation using remote sensing techniques implemented with Landsat series satellites (OLI, ETM+). The conclusions are as follows:

1. In this study, with regard to results of training sample, we observed 21.05% and 23.45% uncertainty in biomass estimation using original images from the OLI and ETM+, respectively. For the test sample, an uncertainty of 33.70% and 34.28% was found, respectively. The three pretreatments can effectively improve the stability of model accuracy. Atmospheric correction was the main process for reducing the uncertainty of remote sensing biomass in the pretreatment stage. In the training sample, this reduced uncertainty by 3.78% and 3.72% for OLI and ETM+, respectively, as opposed to 5.56% and 4.41% in the test sample, Terrain correction can reduce the uncertainty of biomass estimation of OLI (training sample: 1.08%, test sample: 1.00%) and ETM+ (training sample: 2.42%, test sample: 1.67%). On the other hand, radiation calibration will slightly reduce the accuracy of the model and increase the uncertainty of remote sensing biomass estimation (OLI increased by 0.62% and 1.4%, ETM+ increased by 0.94% and 2.1%).
2. Radiometric calibration as well as atmospheric and terrain corrections showed consistent basic characteristics with respect to the uncertainty of biomass estimation using remote sensing in Landsat series satellites (OLI, ETM+). Radiometric calibration can slightly increase the uncertainty, while atmospheric and terrain correction could significantly reduce the uncertainty and with similar effects.
3. Atmospheric correction was a primary means for reducing the uncertainty of biomass estimation during pretreatment, and thus we conclude that the improved atmospheric correction method is beneficial for the further reduction of uncertainty during biomass estimation. However, the influence of solar elevation angle should be considered when performing terrain correction and choosing an appropriate optical image is recommended to improve the predictive accuracy.

We believe that the uncertainty evaluations presented in this study can easily be transferred to the estimation and analysis of biomass data from other space or airborne sensors. Particularly, those evaluations related to the estimation of atmospheric correction will be the main source of uncertainties in the pre-processing phase prior to biomass estimation. This has to be considered deeper in future biomass estimation using remote sensing. In this study, significant efforts in the uncertainty of biomass estimation using Landsat remote sensing have been focused on the pre-processing phase. In the future, we expect new insights into the causes of the uncertainties following radiometric calibration as well as atmospheric and terrain correction.

Author Contributions: Conceptualization, Qi Zhang, Lihua Xu, Maozhen Zhang; Methodology, Qi Zhang, Lihua Xu, Maozhen Zhang; Software, Qi Zhang, Lihua Xu, Maozhen Zhang; Validation, Qi Zhang, Lihua Xu, Maozhen

Zhang; Formal Analysis, Qi Zhang, Lihua Xu, Maozhen Zhang, Zhi Wang, Zhangfeng Gu, Yaqi Wu, Yijun Shi and Zhangwei Lu; Investigation, Maozhen Zhang; Data Curation, Maozhen Zhang; Writing—Original Draft Preparation, Qi Zhang; Writing—Review and Editing, Qi Zhang, Lihua Xu, Maozhen Zhang and Yijun Shi; Administration, Lihua Xu; Funding Acquisition, Lihua Xu. All authors have read and agreed to the published version of the manuscript.

Funding: This study was undertaken with the support of the National Natural Science Foundation of China (No. 41871216).

Acknowledgments: The authors would like to thank the U.S. Geological Survey for providing open-access data.

Conflicts of Interest: The authors declare no conflict of interest.

References

1. Achard, F.; Eva, H.D.; Mayaux, P.; Stibig, H.J.; Belward, A. Improved estimates of net carbon emissions from land cover change in the tropics for the 1990s. *Glob. Biogeochem. Cycles* **2004**, *18*. [[CrossRef](#)]
2. Frohling, S.; Palace, M.W.; Clark, D.B.; Chambers, J.Q.; Shugart, H.H.; Hurtt, G.C. Forest disturbance and recovery: A general review in the context of spaceborne remote sensing of impacts on aboveground biomass and canopy structure. *J. Geophys. Res. Biogeosci.* **2015**, *114*, 544. [[CrossRef](#)]
3. Hansen, M.C.; Potapov, P.V.; Moore, R.; Hancher, M.; Turubanova, S.A.; Tyukavina, A.; Thau, D.; Stehman, S.V.; Goetz, S.J.; Loveland, T.R. High-resolution global maps of 21st-century forest cover change. *Science* **2014**, *342*, 850–853. [[CrossRef](#)] [[PubMed](#)]
4. Houghton, R.A. Aboveground forest biomass and the global carbon balance. *Glob. Chang. Biol.* **2010**, *11*, 945–958. [[CrossRef](#)]
5. Hese, S.; Lucht, W.; Schmillius, C.; Barnsley, M.; Dubayah, R.; Knorr, D.; Neumann, K.; Riedel, T.; Schröter, K. Global biomass mapping for an improved understanding of the co₂ balance—The earth observation mission carbon-3d. *Remote Sens. Environ.* **2005**, *94*, 94–104. [[CrossRef](#)]
6. Sedjo, R.A. The carbon cycle and global forest ecosystem. *Water Air Soil Pollut.* **1993**, *70*, 295–307. [[CrossRef](#)]
7. Waring, R.H.; Running, S.W. *Forest Ecosystems, Analysis at Multiple Scales*, 3rd ed.; Elsevier: Boston, MA, USA; Academic Press: Amsterdam, The Netherlands, 2007; pp. 347–408.
8. Schlamadinger, B.; Marland, G. The role of forest and bioenergy strategies in the global carbon cycle. *Biomass Bioenergy* **1996**, *11*, 275–300. [[CrossRef](#)]
9. Brinck, K.; Fischer, R.; Groeneveld, J.; Lehmann, S.; Dantas, D.P.M.; Pütz, S.; Sexton, J.O.; Song, D.; Huth, A. High resolution analysis of tropical forest fragmentation and its impact on the global carbon cycle. *Nat. Commun.* **2017**, *8*, 14855. [[CrossRef](#)]
10. Gibbs, H.K.; Brown, S.; Niles, J.O.; Foley, J.A. Monitoring and estimating tropical forest carbon stocks: Making redd a reality. *Environ. Res. Lett.* **2007**, *2*, 045023. [[CrossRef](#)]
11. Mandels, M.; Weber, J.; Parizek, R. Realising redd+ national strategy and policy options. *Cent. Int. For. Res.* **2009**, *18*, 6362–6369.
12. Gumpenberger, M.; Vohland, K.; Heyder, U.; Poulter, B.; Macey, K.; Rammig, A.; Popp, A.; Cramer, W. Predicting pan-tropical climate change induced forest stock gains and losses—Implications for REDD. *Environ. Res. Lett.* **2018**, *5*, 014013. [[CrossRef](#)]
13. Galidaki, G.; Zianis, D.; Gitas, I.; Radoglou, K.; Karathanassi, V.; Tsakiri-Strati, M.; Woodhouse, I.; Mallinis, G. Vegetation biomass estimation with remote sensing: Focus on forest and other wooded land over the mediterranean ecosystem. *Int. J. Remote Sens.* **2017**, *38*, 1940–1966. [[CrossRef](#)]
14. Lu, D.; Chen, Q.; Wang, G.; Liu, L.; Li, G.; Moran, E. A survey of remote sensing-based aboveground biomass estimation methods in forest ecosystems. *Int. J. Digit. Earth* **2014**, *9*, 63–105. [[CrossRef](#)]
15. Chave, J.; Réjou-Méchain, M.; Búrquez, A.; Chidumayo, E.; Colgan, M.S.; Delitti, W.B.C.; Duque, A.; Eid, T.; Fearnside, P.M.; Goodman, R.C. Improved allometric models to estimate the aboveground biomass of tropical trees. *Glob. Chang. Biol.* **2015**, *20*, 3177–3190. [[CrossRef](#)] [[PubMed](#)]
16. Alves, L.F.; Vieira, S.A.; Scaranello, M.A.; Camargo, P.B.; Santos, F.A.M.; Joly, C.A.; Martinelli, L.A. Forest structure and live aboveground biomass variation along an elevational gradient of tropical atlantic moist forest (Brazil). *For. Ecol. Manag.* **2010**, *260*, 679–691. [[CrossRef](#)]
17. Kumar, L.; Mutanga, O. Remote sensing of above-ground biomass. *Remote Sens.* **2017**, *9*, 935. [[CrossRef](#)]

18. Oliveras, I.; Anderson, L.O.; Malhi, Y. Application of remote sensing to understanding fire regimes and biomass burning emissions of the tropical andes. *Glob. Biogeochem. Cycles* **2014**, *28*, 480–496. [[CrossRef](#)]
19. Fry, J.C. 2 Direct methods and biomass estimation. *Methods Microbiol.* **1990**, *22*, 41–85.
20. Brown, S.; Gillespie, A.J.; Lugo, A.E. Biomass estimation methods for tropical forests with applications to forest inventory data. *For. Sci.* **1989**, *35*, 881–902.
21. Seidel, D.; Fleck, S.; Leuschner, C.; Hammett, T. Review of ground-based methods to measure the distribution of biomass in forest canopies. *Ann. For. Sci.* **2011**, *68*, 225–244. [[CrossRef](#)]
22. Durante, P.; Martín-Alcón, S.; Gil-Tena, A.; Algeet, N.; Tomé, J.L.; Recuero, L.; Palacios-Orueta, A.; Oyonarte, C. Improving aboveground forest biomass maps: From high-resolution to national scale. *Remote Sens.* **2019**, *11*, 795. [[CrossRef](#)]
23. O'Donnell, J.P.R.; Schalles, J.F. Examination of abiotic drivers and their influence on *Spartina alterniflora* biomass over a twenty-eight year period using Landsat 5 TM satellite imagery of the Central Georgia Coast. *Remote Sens.* **2016**, *8*, 477. [[CrossRef](#)]
24. Lu, D. Aboveground biomass estimation using landsat tm data in the Brazilian amazon. *Int. J. Remote Sens.* **2005**, *26*, 2509–2525. [[CrossRef](#)]
25. Næsset, E.; Gobakken, T.; Bollandsås, O.M.; Gregoire, T.G.; Nelson, R.; Ståhl, G. Comparison of precision of biomass estimates in regional field sample surveys and airborne lidar-assisted surveys in Hedmark county, Norway. *Remote Sens. Environ.* **2013**, *130*, 108–120. [[CrossRef](#)]
26. Onisimo, M.; Elhadi, A.; Cho, A.M. High density biomass estimation for wetland vegetation using worldview-2 imagery and random forest regression algorithm. *Int. J. Appl. Earth Obs. Geoinf.* **2012**, *18*, 399–406.
27. Shi, W. *Principles of Modeling Uncertainties in Spatial Data and Spatial Analyses*; CRC Press: Boca Raton, CA, USA, 2009.
28. Hill, T.C.; Williams, M.; Bloom, A.A.; Mitchard, E.T.; Ryan, C.M. Are inventory based and remotely sensed above-ground biomass estimates consistent? *PLoS ONE* **2013**, *8*, e74170. [[CrossRef](#)]
29. Tjelmeland, S. A model for the uncertainty around the yearly trawl-acoustic estimate of biomass of barents sea capelin, *mallotus villosus* (müller). *ICES J. Mar. Sci.* **2002**, *59*, 1072–1080. [[CrossRef](#)]
30. Yu, F. Aboveground biomass estimation and uncertainties assessing on regional scale with an improved model analysis method. *Hubei For. Sci. Technol.* **2018**, *47*, 1–4.
31. Yu, F.; Yuancai, L.; Weisheng, Z. Uncertainty assessment in regional-scale above ground biomass estimation of Chinese fir. *Sci. Silvae Sin.* **2014**, *50*, 79–86.
32. Kaufman, Y. The effect of subpixel clouds on remote sensing. *Int. J. Remote Sens.* **1987**, *8*, 839–857. [[CrossRef](#)]
33. Arvidson, T.; Goward, S.; Gasch, J.; Williams, D. Landsat-7 long-term acquisition plan radiometry-evolution over time. *Photogramm. Eng. Remote Sens.* **2006**, *72*, 1137–1146. [[CrossRef](#)]
34. Nagol, J.R.; Sexton, J.O.; Kim, D.H.; Anand, A.; Morton, D.; Vermote, E.; Townshend, J.R. Bidirectional effects in landsat reflectance estimates: Is there a problem to solve? *ISPRS J. Photogramm. Remote Sens.* **2015**, *103*, 129–135. [[CrossRef](#)]
35. Roy, D.P.; Ju, J.; Lewis, P.; Schaaf, C.; Gao, F.; Hansen, M.; Lindquist, E. Multi-temporal modis-landsat data fusion for relative radiometric normalization, gap filling, and prediction of landsat data. *Remote Sens. Environ.* **2008**, *112*, 3112–3130. [[CrossRef](#)]
36. Steven, M.D.; Malthus, T.J.; Baret, F.; Hui, X.; Chopping, M.J. Intercalibration of vegetation indices from different sensor systems. *Remote Sens. Environ.* **2003**, *88*, 412–422. [[CrossRef](#)]
37. Tucker, C.J.; Pinzon, J.E.; Brown, M.E.; Slayback, D.A.; Pak, E.W.; Mahoney, R.; Vermote, E.F.; Saleous, N.E. An extended AVHRR 8-km NDVI dataset compatible with MODIS and SPOT vegetation NDVI data. *Int. J. Remote Sens.* **2005**, *26*, 4485–4498. [[CrossRef](#)]
38. Roy, D.P.; Borak, J.S.; Devadiga, S. The modis land product quality assessment approach. *Remote Sens. Environ.* **2002**, *83*, 62–76. [[CrossRef](#)]
39. Roy, D.P.; Kovalsky, V.; Zhang, H.K.; Vermote, E.F.; Yan, L.; Kumar, S.S.; Egorov, A. Characterization of landsat-7 to landsat-8 reflective wavelength and normalized difference vegetation index continuity. *Remote Sens. Environ.* **2016**, *185*, 57–70. [[CrossRef](#)]
40. Chave, J.; Davies, S.J.; Phillips, O.L.; Lewis, S.L.; Sist, P.; Schepaschenko, D.; Armston, J.; Baker, T.R.; Coomes, D.; Disney, M. Ground data are essential for biomass remote sensing missions. *Surv. Geophys.* **2019**. [[CrossRef](#)]

41. Van, B.M.; Ransijn, J.; Craven, D.; Bongers, F.; Hall, J.S. Estimating carbon stock in secondary forests: Decisions and uncertainties associated with allometric biomass models. *For. Ecol. Manag.* **2011**, *262*, 1648–1657.
42. Sándor, R.; Barcza, Z.; Acutis, M.; Doro, L.; Hidy, D.; Köchy, M.; Minet, J.; Lellei-Kovács, E.; Ma, S.; Perego, A. Multi-model simulation of soil temperature, soil water content and biomass in euro-mediterranean grasslands: Uncertainties and ensemble performance. *Eur. J. Agron.* **2017**, *88*, 22–40. [[CrossRef](#)]
43. Breidenbach, J.; Antón-Fernández, C.; Petersson, H.; Mcroberts, R.E.; Astrup, R. Quantifying the model-related variability of biomass stock and change estimates in the norwegian national forest inventory. *For. Sci.* **2014**, *60*, 25–33. [[CrossRef](#)]
44. Lu, D.; Chen, Q.; Wang, G.; Moran, E.; Saah, D. Aboveground forest biomass estimation with landsat and lidar data and uncertainty analysis of the estimates. *Int. J. For. Res.* **2012**, *2012*, 436537. [[CrossRef](#)]
45. Molto, Q.; Rossi, V.; Blanc, L. Error propagation in biomass estimation in tropical forests. *Methods Ecol. Evol.* **2013**, *4*, 175–183. [[CrossRef](#)]
46. Frazer, G.W.; Magnussen, S.; Wulder, M.A.; Niemann, K.O. Simulated impact of sample plot size and co-registration error on the accuracy and uncertainty of lidar-derived estimates of forest stand biomass. *Remote Sens. Environ.* **2011**, *115*, 636–649. [[CrossRef](#)]
47. Keller, M.; Palace, M.; Hurtt, G. Biomass estimation in the Tapajos National Forest, Brazil: Examination of sampling and allometric uncertainties. *For. Ecol. Manag.* **2001**, *154*, 371–382. [[CrossRef](#)]
48. Samimi, C.; Kraus, T. Biomass estimation using landsat-tm and -etm+. Towards a regional model for southern Africa? *GeoJournal* **2004**, *59*, 177–187. [[CrossRef](#)]
49. Zheng, D.; Rademacher, J.; Chen, J.; Crow, T.; Bresee, M.; Moine, J.L.; Ryu, S.R. Estimating aboveground biomass using landsat 7 etm+ data across a managed landscape in northern wisconsin, USA. *Remote Sens. Environ.* **2004**, *93*, 402–411. [[CrossRef](#)]
50. Chenge, I.B.; Osho, J.S. Mapping tree aboveground biomass and carbon in omo forest reserve Nigeria using landsat 8 oli data. *South. For.* **2018**, *80*, 1–10. [[CrossRef](#)]
51. Belachew, G.; Svein, S.; Erik, N.; Terje, G.; Martin, B.O.; Johannes, B.; Eliakimu, Z.; William, M.E. Mapping and estimating the total living biomass and carbon in low-biomass woodlands using landsat 8 cdr data. *Carbon Balance Manag.* **2016**, *11*, 13.
52. Mira, M.; Olioso, A.; Gallego-Elvira, B.; Courault, D.; Garrigues, S.; Marloie, O.; Hagolle, O.; Guillevic, P.; Boulet, G. Uncertainty assessment of surface net radiation derived from landsat images. *Remote Sens. Environ.* **2016**, *175*, 251–270. [[CrossRef](#)]
53. Gertner, G.; Wang, G.; Fang, S.; Anderson, A.B. Mapping and uncertainty of predictions based on multiple primary variables from joint co-simulation with landsat tm image and polynomial regression. *Remote Sens. Environ.* **2002**, *83*, 498–510. [[CrossRef](#)]
54. Fleming, A.L.; Wang, G.; Mcroberts, R.E. Comparison of methods toward multi-scale forest carbon mapping and spatial uncertainty analysis: Combining national forest inventory plot data and landsat tm images. *Eur. J. For. Res.* **2015**, *134*, 125–137. [[CrossRef](#)]
55. Sánchez, J.M. Validation of landsat-7/etm+ thermal-band calibration and atmospheric correction with ground-based measurements. *IEEE Trans. Geosci. Remote Sens.* **2010**, *48*, 547–555.
56. Thome, K.J. Absolute radiometric calibration of landsat 7 etm+ using the reflectance-based method. *Remote Sens. Environ.* **2001**, *78*, 27–38. [[CrossRef](#)]
57. Campbell, J.B. *Introduction to Remote Sensing*; The Guilford Press: New York, NY, USA; London, UK, 1987; pp. 51–67.
58. Markham, B.; Barsi, J.; Kvaran, G.; Ong, L.; Helder, D. Landsat-8 operational land imager radiometric calibration and stability. *Remote Sens.* **2014**, *6*, 12275–12308. [[CrossRef](#)]
59. Zhang, W.; Yu, D.; Shi, X.; Zhang, X.; Wang, H.; Gu, Z. Uncertainty in prediction of soil erodibility k-factor in subtropical china. *Acta Pedol. Sin.* **2009**, *46*, 185–191.
60. He, L. A Study on the Uncertainty of Regional Winter Wheat Growth Simulation from a Crop model Using Remote Sensing Data Assimilation. Ph.D. Thesis, Chinese Academy of Agricultural Sciences, Beijing, China, June 2016.
61. Zeng, W.; Tomppo, E.; Healey, S.P.; Gadov, K.V. The national forest inventory in china: History-results-international context. *For. Ecosyst.* **2015**, *2*, 23. [[CrossRef](#)]
62. Fang, J.; Oikawa, T.; Kato, T.; Mo, W.; Wang, Z. Biomass carbon accumulation by Japan's forests from 1947 to 1995. *Glob. Biogeochem. Cycles* **2005**, *19*. [[CrossRef](#)]

63. Tomppo, E.; Olsson, H.; Ståhl, G.; Nilsson, M.; Hagner, O.; Katila, M. Combining national forest inventory field plots and remote sensing data for forest databases. *Remote Sens. Environ.* **2008**, *112*, 1982–1999. [[CrossRef](#)]
64. Nilsson, M.; Nordkvist, K.; Jonzén, J.; Lindgren, N.; Axensten, P.; Wallerman, J.; Egberth, M.; Larsson, S.; Nilsson, L.; Eriksson, J. A nationwide forest attribute map of Sweden predicted using airborne laser scanning data and field data from the national forest inventory. *Remote Sens. Environ.* **2017**, *194*, 447–454. [[CrossRef](#)]
65. Guo, Z.; Fang, J.; Pan, Y.; Birdsey, R. Inventory-based estimates of forest biomass carbon stocks in china: A comparison of three methods. *For. Ecol. Manag.* **2010**, *259*, 1225–1231. [[CrossRef](#)]
66. Brown, S.; Lugo, A.E. Biomass of tropical forests: A new estimate based on forest volumes. *Science* **1984**, *223*, 1290–1293. [[CrossRef](#)] [[PubMed](#)]
67. Birdsey, R.; Heath, L. Forest inventory data, models, and assumptions for monitoring carbon flux. *SSSA Spec. Publ.* **2001**, *57*, 125–136.
68. Canadell, J.G.; Le Quéré, C.; Raupach, M.R.; Field, C.B.; Buitenhuis, E.T.; Ciais, P.; Conway, T.J.; Gillett, N.P.; Houghton, R.; Marland, G. Contributions to accelerating atmospheric CO₂ growth from economic activity, carbon intensity, and efficiency of natural sinks. *Proc. Natl. Acad. Sci. USA* **2007**, *104*, 18866–18870. [[CrossRef](#)] [[PubMed](#)]
69. Piao, S.; Fang, J.; Zhu, B.; Tan, K. Forest biomass carbon stocks in china over the past 2 decades: Estimation based on integrated inventory and satellite data. *J. Geophys. Res. Biogeosci.* **2005**, *110*. [[CrossRef](#)]
70. Du, L.; Zhou, T.; Zou, Z.; Zhao, X.; Huang, K.; Wu, H. Mapping forest biomass using remote sensing and national forest inventory in China. *Forests* **2014**, *5*, 1267–1283. [[CrossRef](#)]
71. Breiman, L. Random forests. *Mach. Learn.* **2001**, *45*, 5–32. [[CrossRef](#)]
72. Barbosa, J.; Broadbent, E.; Bitencourt, M. Remote sensing of aboveground biomass in tropical secondary forests: A review. *Int. J. For. Res.* **2014**, *2014*, 715796. [[CrossRef](#)]
73. Kamusoko, C.; Jonah, G.; Murakami, H. Mapping woodland cover in the miombo ecosystem: A comparison of machine learning classifiers. *Land* **2014**, *3*, 524–540. [[CrossRef](#)]
74. Coulston, J.W.; Blinn, C.E.; Thomas, V.A.; Wynne, R.H. Approximating prediction uncertainty for random forest regression models. *Photogramm. Eng. Remote Sens.* **2016**, *82*, 189–197. [[CrossRef](#)]
75. Powell, S.L.; Cohen, W.B.; Healey, S.P.; Kennedy, R.E.; Moisen, G.G.; Pierce, K.B.; Ohmann, J.L. Quantification of live aboveground forest biomass dynamics with landsat time-series and field inventory data: A comparison of empirical modeling approaches. *Remote Sens. Environ.* **2010**, *114*, 1053–1068. [[CrossRef](#)]
76. Ismail, R.; Mutanga, O.; Woldai, T.; Annegarn, H. A comparison of regression tree ensembles: Predicting siresx noctilio induced water stress in pinus patula forests of kwazulu-natal, South Africa. *Int. J. Appl. Earth Obs. Geoinf.* **2010**, *12*, S45–S51. [[CrossRef](#)]
77. Liaw, A.; Wiener, M. Classification and regression by randomforest. *R News* **2002**, *2*, 18–22.
78. Rouse, J.W., Jr.; Haas, R.H.; Schell, J.A.; Deering, D.W. Monitoring Vegetation Systems in the Great Plains with ERTS. In Proceedings of the Third ERTS-1 Symposium NASA, NASA SP-351, Washington, DC, USA, 29 September 1974; pp. 812–815.
79. Gitelson, A.A.; Kaufman, Y.J.; Merzlyak, M.N. Use of a green channel in remote sensing of global vegetation from eos-modis. *Remote Sens. Environ.* **1996**, *58*, 289–298. [[CrossRef](#)]
80. Huete, A.R. A soil-adjusted vegetation index (savi). *Remote Sens. Environ.* **1988**, *25*, 295–309. [[CrossRef](#)]
81. Qi, J.; Huete, A.; Moran, M.S.; Chehbouni, A.; Jackson, R.D. Interpretation of vegetation indices derived from multi-temporal spot images. *Remote Sens. Environ.* **1993**, *44*, 89–101. [[CrossRef](#)]
82. Liu, H.Q.; Huete, A. A feedback based modification of the ndvi to minimize canopy background and atmospheric noise. *IEEE Trans. Geosci. Remote Sens.* **1995**, *33*, 457–465. [[CrossRef](#)]
83. Fassnacht, F.E.; Hartig, F.; Latifi, H.; Berger, C.; Hernández, J.; Corvalán, P.; Koch, B. Importance of sample size, data type and prediction method for remote sensing-based estimations of aboveground forest biomass. *Remote Sens. Environ.* **2014**, *154*, 102–114. [[CrossRef](#)]
84. Yang, Y.; Cao, C.; Pan, X.; Li, X.; Zhu, X. Downscaling land surface temperature in an arid area by using multiple remote sensing indices with random forest regression. *Remote Sens.* **2017**, *9*, 789. [[CrossRef](#)]
85. Sun, X.; Lin, X.; Shen, S.; Hu, Z. High-resolution remote sensing data classification over urban areas using random forest ensemble and fully connected conditional random field. *ISPRS Int. J. Geo Inf.* **2017**, *6*, 245. [[CrossRef](#)]

86. Shen, R.; Guo, J.; Zhang, J.; Luoxi, L.I. Construction of a drought monitoring model using the random forest based remote sensing. *J. Geo-Inf. Sci.* **2017**, *19*, 125–133.
87. Mishra, N.; Helder, D.; Barsi, J.; Markham, B. Continuous calibration improvement in solar reflective bands: Landsat 5 through landsat 8. *Remote Sens. Environ.* **2016**, *185*, 7–15. [[CrossRef](#)] [[PubMed](#)]
88. Ghulam, A.; Qin, Q.; Zhu, L.; Abdrahman, P. Satellite remote sensing of groundwater: Quantitative modelling and uncertainty reduction using 6s atmospheric simulations. *Int. J. Remote Sens.* **2004**, *25*, 5509–5524. [[CrossRef](#)]
89. Sarker, L.R.; Nichol, J.E. Improved forest biomass estimates using alos avnir-2 texture indices. *Remote Sens. Environ.* **2011**, *115*, 968–977. [[CrossRef](#)]
90. Hieu Cong, N.; Jaehoon, J.; Jungbin, L.; Sung-Uk, C.; Suk-Young, H.; Joon, H. Optimal atmospheric correction for above-ground forest biomass estimation with the etm+ remote sensor. *Sensors* **2015**, *15*, 18865–18886.
91. Zhu, W.; Huang, L.; Sun, N.; Chen, J.; Pang, S. Landsat 8-observed water quality and its coupled environmental factors for urban scenery lakes: A case study of west lake. *Water Environ. Res.* **2019**. [[CrossRef](#)]
92. Deo, R.K.; Domke, G.M.; Russell, M.B.; Woodall, C.W.; Andersen, H.E. Evaluating the influence of spatial resolution of landsat predictors on the accuracy of biomass models for large-area estimation across the eastern USA. *Environ. Res. Lett.* **2018**, *13*, 055004. [[CrossRef](#)]
93. Chave, J.; Chust, G.; Condit, R.; Aguilar, S.; Hernandez, A.; Lao, S.; Perez, R. Error propagation and scaling for tropical forest biomass estimates. *Philos. Trans. R Soc. Lond. B Biol. Sci.* **2004**, *359*, 409–420. [[CrossRef](#)]
94. Baker, D.J.; Richards, G.; Grainger, A.; Gonzalez, P.; Brown, S.; Defries, R.; Held, A.; Kellndorfer, J.; Ndunda, P.; Ojima, D. Achieving forest carbon information with higher certainty: A five-part plan. *Environ. Sci. Policy* **2010**, *13*, 249–260. [[CrossRef](#)]



© 2020 by the authors. Licensee MDPI, Basel, Switzerland. This article is an open access article distributed under the terms and conditions of the Creative Commons Attribution (CC BY) license (<http://creativecommons.org/licenses/by/4.0/>).